

Molecular imaging by Mid-IR laser ablation mass spectrometry

Akos Vertes · Peter Nemes · Bindesh Shrestha ·
Alexis A. Barton · Zhaoyang Chen · Yue Li

Received: 12 October 2007 / Accepted: 9 April 2008 / Published online: 4 July 2008
© Springer-Verlag 2008

Abstract Mid-IR laser ablation at atmospheric pressure (AP) produces a mixture of ions, neutrals, clusters, and particles with a size distribution extending into the nanoparticle range. Using external electric fields the ions can be extracted and sampled by a mass spectrometer. In AP infrared (IR) matrix-assisted laser desorption ionization (MALDI) experiments, the plume was shown to contain an appreciable proportion of ionic components that reflected the composition of the ablated target and enabled mass spectrometric analysis. The detected ion intensities rapidly declined with increasing distance of sampling from the ablated surface to ~ 4 mm. This was rationalized in terms of ion recombination and the stopping of the plume expansion by the background gas. In laser ablation electrospray ionization (LAESI) experiments, the ablation plume was intercepted by an electrospray. The neutral particles in the plume were ionized by the charged droplets in the spray and enabled the detection of large molecules (up to 66 kDa). Maximum ion production in LAESI was observed at large (~ 15 mm) spray axis to ablated surface distance indicating a radically different ion formation mechanism compared to AP IR-MALDI. The feasibility of molecular imaging by both AP IR-MALDI and LAESI was demonstrated on targets with mock patterns.

PACS 52.38.Mf · 79.20.Ds · 82.80.Ms

Presented at the 9-th International Conference on Laser Ablation, 2007 Tenerife, Canary Islands, Spain

A. Vertes (✉) · P. Nemes · B. Shrestha · A.A. Barton · Z. Chen · Y. Li
Department of Chemistry, George Washington University,
725 21st Street, N.W., Washington, DC 20052, USA
e-mail: vertes@gwu.edu

1 Introduction

In recent years atmospheric pressure (AP) laser ablation has been increasingly used in chemical analysis. As its vacuum counterpart, AP laser ablation can be utilized to produce ions, neutrals, clusters, nanoparticles and particulate matter from diverse targets. Depending on the applied laser wavelength, pulse duration and fluence and on the properties of the target and the background gas, the relative amount and the nature of these species may be vastly different. The laser-target interactions exhibit numerous regimes that are governed by the prevailing energy deposition, redistribution and dissipation mechanisms. Due to its low ion yield, preferential evaporation and ionization, direct AP laser ablation has rarely been used for chemical analysis. Instead, the established methods rely on converting other species in the laser plume into detectable ions.

In elemental analysis the combination of AP laser ablation with inductively coupled plasma mass spectrometry proved itself valuable for the microanalysis of solids [1, 2]. This high energy postionization method is based on converting neutrals, clusters and particles into elemental ions in a high temperature plasma supported by radio frequency current. In molecular analysis, the emerging methods include AP matrix-assisted laser desorption ionization (MALDI) mass spectrometry using ultraviolet (UV) [3, 4] and infrared (IR) lasers [5, 6]. These methods rely on the presence of an energy absorbing matrix material that dramatically enhances the coupling of the laser energy into the target. While these techniques improved the ease of analysis for broad sample classes (including *in vivo* analysis), persistent debates about their lower sensitivity and especially their reduced high-mass limits compared to the corresponding vacuum methods continued to limit their acceptance. For

example, AP IR-MALDI mass analysis of a peptide mixture containing bradykinin (m/z 1060.4), substance P (m/z 1347.6), and insulin (m/z 5733.5) showed discrimination against $m/z > 3,000$ ions [7].

Although it is known from vacuum MALDI studies that both the UV and the IR laser ablation plume may contain ions from large molecules ($m/z > 100,000$), the ion yield is known to be 10^{-4} or less even for small molecules at the laser fluence threshold for ion generation [8]. As this number results from postionization experiments based on photoexcitation, it is an upper limit for the degree of ionization, because it does not account for the extensive amount of neutrals ablated as nanoparticles and particulate matter [9]. Further factors that limit the efficiency of ion detection are the enhanced recombination of the laser generated ions in the expanding plume under AP conditions [10, 11] and the limited ion collection efficiency of the mass spectrometer [12]. Clearly, efficient but gentle postionization is necessary to improve the ion yield in these experiments without extensive fragmentation and plasma formation.

Although postionization in vacuum environment based on a second laser beam that intercepts the ablation plume produced by the first laser has a long history (see e.g. [13–17]), the application of this technique at atmospheric pressure has not been explored. Furthermore, the results in the vacuum experiments indicate that the overall gain in the total ion yield is modest, probably due to the inability of the postionization laser to efficiently disperse and ionize the clusters, nanoparticles and particulate matter in the plume. Postionization of the ablated plume at atmospheric pressure is much less studied. Recent advances in photoionization [18] and chemical ionization of the ablated material using reactive ions produced by a corona discharge indicate an increase of up to two orders of magnitude in the ionization efficiency [19, 20]. In a different approach, the laser ablation plume was intercepted by an electrospray plume to achieve ion production from nanoparticles and particulates produced by UV [21, 22] and IR [23] lasers. This latter method, termed laser ablation electrospray ionization (LAESI), proved to be capable of *in vivo* analysis of plant organs as well as direct analysis of biological fluids.

In this contribution we compare ion production in AP IR-MALDI and in LAESI from diverse targets, including plant organs and bodily fluids. Optimization of ion sampling in the two methods reveals some of their mechanistic differences. Molecular imaging capabilities are demonstrated for both methods.

2 Experimental

The two experimental arrangements used in this study are shown in Fig. 1. Both the AP IR-MALDI and the LAESI

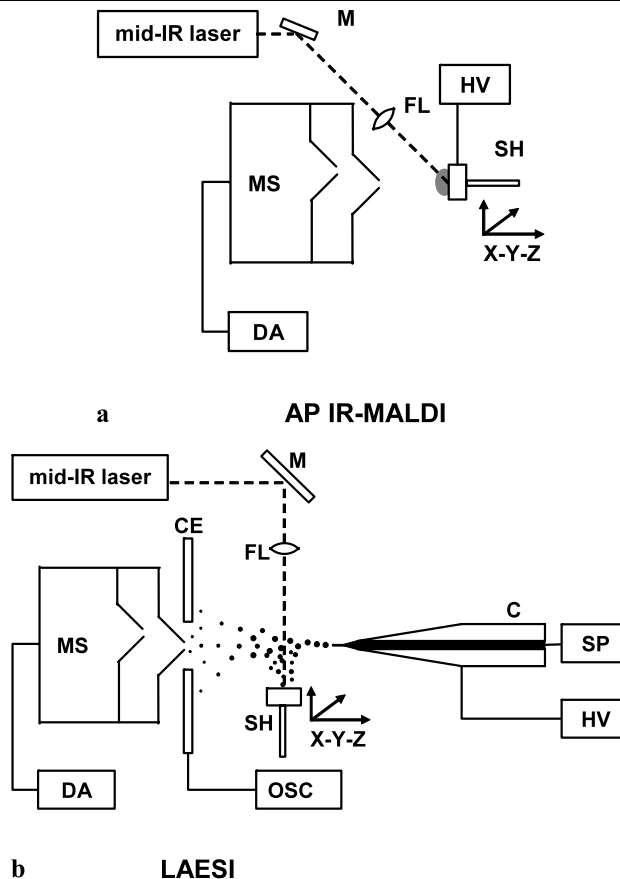


Fig. 1 Schematics of two atmospheric pressure IR laser ablation systems used in biomedical analysis based on **a** the AP IR-MALDI and **b** the LAESI configuration. System components include C—capillary; SP—syringe pump; HV—high-voltage power supply; M—mirror; FL—focusing lens; CE—counter electrode; OSC—digital oscilloscope; SH—sample holder; X-Y-Z—motorized micropositioning system; mid-IR laser—Nd:YAG laser driven OPO or Er:YAG laser; MS—mass spectrometer; and DA—data acquisition system

system have been described in detail elsewhere (see [7] and [23], respectively). Briefly, laser ablation was achieved by a Nd:YAG laser driven optical parametric oscillator (OPO) (Vibrant IR, Oportek Inc., Carlsbad, CA) and in some LAESI experiments by an Er:YAG laser. The radiation at 2940 nm wavelength from the OPO source had a pulse length of 4 ns, whereas the Er:YAG laser produced 100 ns pulses. In the AP IR-MALDI experiments the elliptical focal spots resulting from the 45° angle of incidence exhibited 200 μm and 650 μm small and large axes, respectively. In the LAESI configuration the laser pulses impinged on the target surface under a right angle and circular focal spots were produced with 350–400 μm diameter. The laser fluences produced at the target were 0.3–1.0 J/cm^2 for the AP IR-MALDI and 0.8–3.6 J/cm^2 for the LAESI experiments.

Two orthogonal acceleration time-of-flight (oa-TOF) mass spectrometers, an AccuTOF (JEOL, Peabody, MA) and a Q-TOF Premier (Waters Co., Milford, MA), were used

to detect the ions. The initial LAESI experiments were performed on the AccuTOF system in combination with the Er:YAG laser. For tandem mass spectrometry used to study the structure of unknown ions and for LAESI imaging, the Q-TOF mass spectrometer was equipped with the OPO laser source. All the AP IR-MALDI experiments were performed on the latter system.

For the molecular imaging experiments, the sample holder was mounted on a NanoMax TS motorized positioning stage. Imaging was achieved by scanning the target in the X-Y plane with a travel range of 4 mm in both directions. Positioning in the Z direction for signal optimization was achieved with a manual translation stage.

In the LAESI experiments, a home-built electrospray source was used for postionization. Details of this source are available in [24]. For best performance, that is, for the highest postionization yield, the 100 μm i.d. and 320 μm o.d. tapered tip metal emitter (New Objective, Woburn, MA) was operated in the cone-jet mode. The spraying mode was monitored through the spray current measured on the stainless steel counter electrode using a digital oscilloscope. A sprayed 50% methanol solution containing 0.1% (v/v) acetic acid was supplied by a syringe pump.

3 Results and discussion

3.1 Direct and postionization in the ablation plume

Based on the two experimental configurations in Fig. 1, we compare the travel range of ions and neutral particles produced by the mid-IR laser ablation. The AP IR-MALDI system enables us to monitor the directly produced ion abundances as a function of the distance between the ablation site on the target surface and the inlet orifice of the mass spectrometer. The neutral particles can be postionized by the electrospray plume in the LAESI configuration. By changing the distance between the ablation site on the target and the axis of the electrospray plume, the travel range of the most efficiently ionized particles may be determined.

Studies on the AP mid-IR laser ablation of biological tissues indicate the presence of two phases [25, 26]. In the early phase of the ablation (first 1 to 2 μs), vaporization of the water and the biomolecules from the tissue produces a hemispherical plume that exhibits partial ionization. This expanding plume drives a shock wave at its interface with the background gas. Eventually the energy of this plume dissipates through the work exerted on the background gas and its expansion is stopped [27]. Most of the ion content of this plume neutralizes through recombination.

An indication of plume stopping is the rapid decline of ion collection as the sampling orifice of the mass spectrometer is moved away from the target surface. Typical stopping distances in our experiments were 2 to 4 mm depending on the laser fluence. The curve labeled AP IR-MALDI in

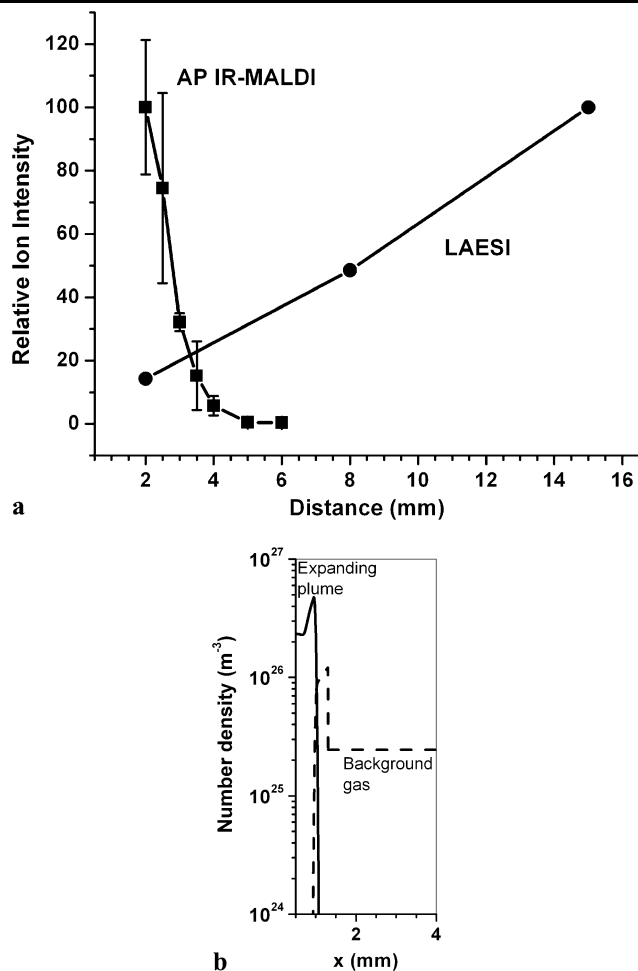


Fig. 2 **a** Relative ion intensities in AP IR-MALDI as a function of sampling orifice distance from the surface and in LAESI as a function of the vertical position where the spray axis intercepts the laser ablation plume. **b** Plume number density distributions for 1.4 J/cm^2 Er:YAG laser ablation of water into 1 atm nitrogen gas at 800 ns. The expanding plume distribution (solid line) shows a high density region close to the shock front and the pile-up of background gas (dashed line) in front of the interface

Fig. 2a shows the precipitous decline of the relative ion intensity for protonated bradykinin molecules produced from 2,5-dihydroxybenzoic acid (DHB) matrix. The OPO was tuned to 2940 nm to deliver 0.58 mJ pulses at 10 Hz repetition rate to a ~ 300 μm diameter area on the target surface, which corresponded to an 0.8 J/cm^2 fluence. The highest ion intensities were detected at a minimum distance of 2 mm from the target. The standoff of the mass spectrometer was not reduced further to avoid electrical breakdown between the target held at +3000 V and the sampling cone held at -55 V. As the sampling distance from the surface increased to 4 mm the relative ion intensity dropped to $\sim 6\%$ of the value at 2 mm.

Using a one dimensional fluid dynamic model to describe the competition of surface evaporation and phase explosion [26], we followed the plume density distributions in the mid-

IR laser ablation of water. Figure 2b shows the shock wave at the water plume background gas (nitrogen) interface at 800 ns into the expansion. At the position of the large density gradient, ~ 1 mm above the surface, the water vapor density dramatically drops and the background gas density rises. Due to the so called “snowplow effect” in front of the vapor plume the background gas density is elevated in a thin layer. This early phase of the plume development is terminated when the displacement of this interface stops and the vapor plume dissipates.

Depending on target properties, the early phase is followed by the expulsion of neutral nanoparticles and small particulates driven by phase explosion and the following recoil pressure induced ejection. This ejection process can last for hundreds of microseconds. Due to the momentum of the ejected particles, this second phase produces a plume with significantly extended range. Although no data are available on how far these particles travel, they are expected to be projected beyond ~ 10 mm above the surface.

The results of our LAESI experiments indicate that ion production through the interaction of the electrospray plume and the laser ablation plume steadily increases as the ablation spot is moved away from the common axis of the spray and the mass spectrometer. The ablation axis, positioned ~ 4 mm ahead of the emitter tip, was perpendicular to the spray axis. The strongest signal for a hemoglobin alpha chain carrying 15 charges produced from human blood was detected with the spray axis at 15 mm above the ablated surface (see the curve labeled LAESI in Fig. 2a). Further increase of the distance resulted in a declining ion signal (not shown), but ions were produced as far as 30 mm away from the ablated surface. Although the IR matrixes of the target material are different (DHB vs. water), the disparate travel range of the ablation produced ions and the ejected particles is obvious in Fig. 2a. While the laser produced ions traveling with the vapor plume almost completely disappear by the time the plume reaches ~ 4 mm, the ion yield from neutral particles increases in this range.

The decrease in AP IR-MALDI signal with the sampling distance can be explained by the combined effect of recombination and the arresting of the plume expansion. The positive ions detected in this experiment efficiently recombine with the electrons and the negative ions in the plume. The presence of these processes is indicated by the strong effect of the target potential on the detected ion signal. When the target potential was lowered close to ground, the ion signal disappeared. A sufficiently high target potential separates the charges in the plume and, in combination with the gas dynamics in the region, guides the extracted positive ions toward the sampling orifice. Recombination in the plume can also explain the bias against large molecules ($m/z > 3000$) in the AP IR-MALDI detection [7]. As the reaction cross section of the positive ions scales with their size, preferential recombination of large ions is expected. This effect

in combination with the declining performance of the ion transfer optics at higher masses in our mass spectrometer can account for the lack of m/z 3000 ions in the observed AP IR-MALDI spectra.

The dynamics of the ejected neutral particles is significantly different. Their trajectories are governed by the dissipation of the initial kinetic energy due to the drag force in the background gas. The initial particle velocities can be several hundreds m/s [25]. From the growing trend of the detected ion intensity with increasing intercept distance in Fig. 2a it can be inferred that this velocity is too high for efficient interaction with the charged droplets in the electrospray. As the particles are slowed down by the drag force, the efficiency of the coalescence increases. Alternatively, the optimum spatial overlap between the laser ablation plume and the electrospray plume can also account for the highest ion signal observed at 15 mm.

The small particles captured by the charged droplets are efficiently dissolved or their soluble components are extracted by the droplet. These charged droplets, seeded by the particles, undergo Coulomb fission and eventually produce ions from the constituents of the ablated particles. This ion production follows the rules of electrospray ionization and, for example, generates multiply charged ions from large molecules of up to 66 kDa molecular weight.

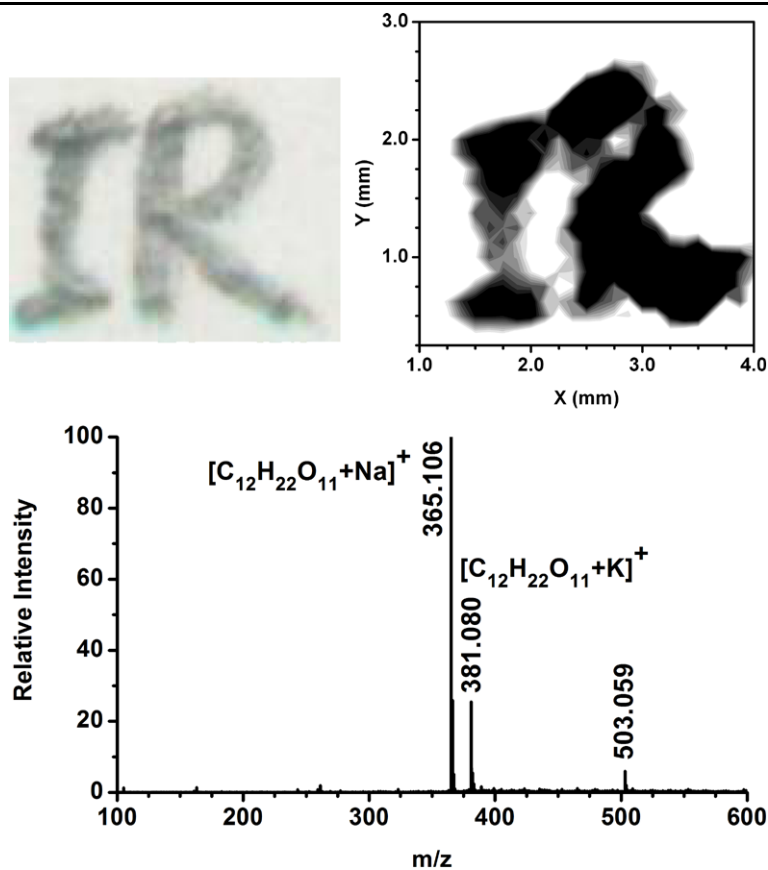
As in LAESI the sampled ablation products are neutral, there is no need to bias the target, and the deleterious effect of recombination does not affect ion production. The ion yield in LAESI strongly depends on the properties of the spray plume (spray plume density and duty cycle, as well as droplet size and composition). For example, maintaining the spray in the cone-jet mode significantly improved the ion yield compared to pulsating spraying modes [23, 24].

3.2 AP IR-MALDI and LAESI imaging

Lateral scanning of patterned targets in front of the laser beam produced position dependent mass spectra with both methods. To show the feasibility of molecular imaging with LAESI and to compare its capabilities with AP IR-MALDI, mock patterns were created and studied.

For the AP IR-MALDI imaging, a graphite pencil was used to write the letters “IR” on a white adhesive paper label (Fisher Scientific). The top left panel in Fig. 3 shows the optical image of the pattern before rastering the surface with the laser. The collected mass spectra showed three prominent peaks in the areas marked by the pencil (bottom panel). Two of the three ions, m/z 365 and 381, were identified as a sodiated and a potassiated disaccharide ($C_{12}H_{22}O_{11}$), respectively [28]. To produce the molecular image of a 4×4 mm² area, spectra were collected on a 33×33 grid with a 125 μ m step size in both directions. The image constructed from the intensity of the m/z 365 ions as a function

Fig. 3 AP IR-MALDI imaging of mock pattern produced by pencil on paper. The optical image (*top left*) shows the letters “IR” before rastering the surface with the laser. Chemical image (*top right*) constructed from the intensity of m/z 365 ions as a function of position on the surface. A typical mass spectrum is shown in the *bottom panel*. The ions m/z 365 and 381 correspond to a sodiated and a potassiumated disaccharide, respectively



of position on the surface is shown in the top right panel. The correlation between the optical and the molecular image is acceptable.

The resolution of the molecular image is limited by the laser focal spot size. The extent of the focal area is currently defined by the properties of the focusing optics (focal length, numerical aperture and spherical aberration) and, more importantly, by the wavelength and the divergence of the laser beam. In future refined versions of the system, a beam expander could significantly reduce the latter and help to produce a significantly smaller focal spot.

For the LAESI imaging experiment [29] a mock pattern of two lines was produced by red (vertical line) and blue (horizontal line) permanent markers (Sharpie, Sanford Co.) on an Peace lily (*Spathiphyllum*) leaf (see the left panel of Fig. 4). In this arrangement the laser beam aligned perpendicular to the target surface illuminated the leaf with an 0.8 J/cm² fluence and produced a circular crater of 350 μm in diameter. Mass spectra were collected on an 11 × 11 grid with a 400 μm step size to produce molecular images in a 4 × 4 mm² area. The collected mass spectra showed the typical ions of primary and secondary metabolites found in leaves and, where marked, the cations from the two dyes. Spectra corresponding to the red vertical line exhibited the m/z 443 species corresponding to the $[C_{28}H_{31}N_2O_3]^+$

cation of the Rhodamine 6G ionic dye. When the sampled areas overlapped with the blue horizontal line, the m/z 478 species was observed, consistent with the $[C_{33}H_{40}N_3]^+$ cation of the Basic Blue 7 common cationic dye. The molecular images for the m/z 443 and 478 ions are shown in the top and bottom middle panels of Fig. 4, respectively. A comparison of the optical and molecular images showed good agreement. Very importantly, in the center where the two lines intercept the cations of both dyes are present in the spectra along with the plant metabolites. Furthermore, the unmarked areas on the leaf also produced metabolite ions indicating the presence of a true chemical contrast.

Inspection of the leaf after the LAESI experiment revealed the presence of tissue damage. The optical image of the exposed area is shown in the right panel of Fig. 4. Although the array of ablation craters can be damaging to small organisms, larger ones can remain viable after a LAESI imaging experiment. Thus, in principle, LAESI is capable of *in vivo* analysis and ultimately molecular imaging. The extent of tissue damage largely depends on the focal spot size. Similarly to AP IR-MALDI, the spatial resolution is also limited by the size of the ablation crater. Reducing the laser focal spot size while maintaining the sensitivity of the method is an important challenge in achieving these goals. Comparing the absolute ion counts on similar samples studied by AP IR-MALDI and LAESI indicates that the lat-

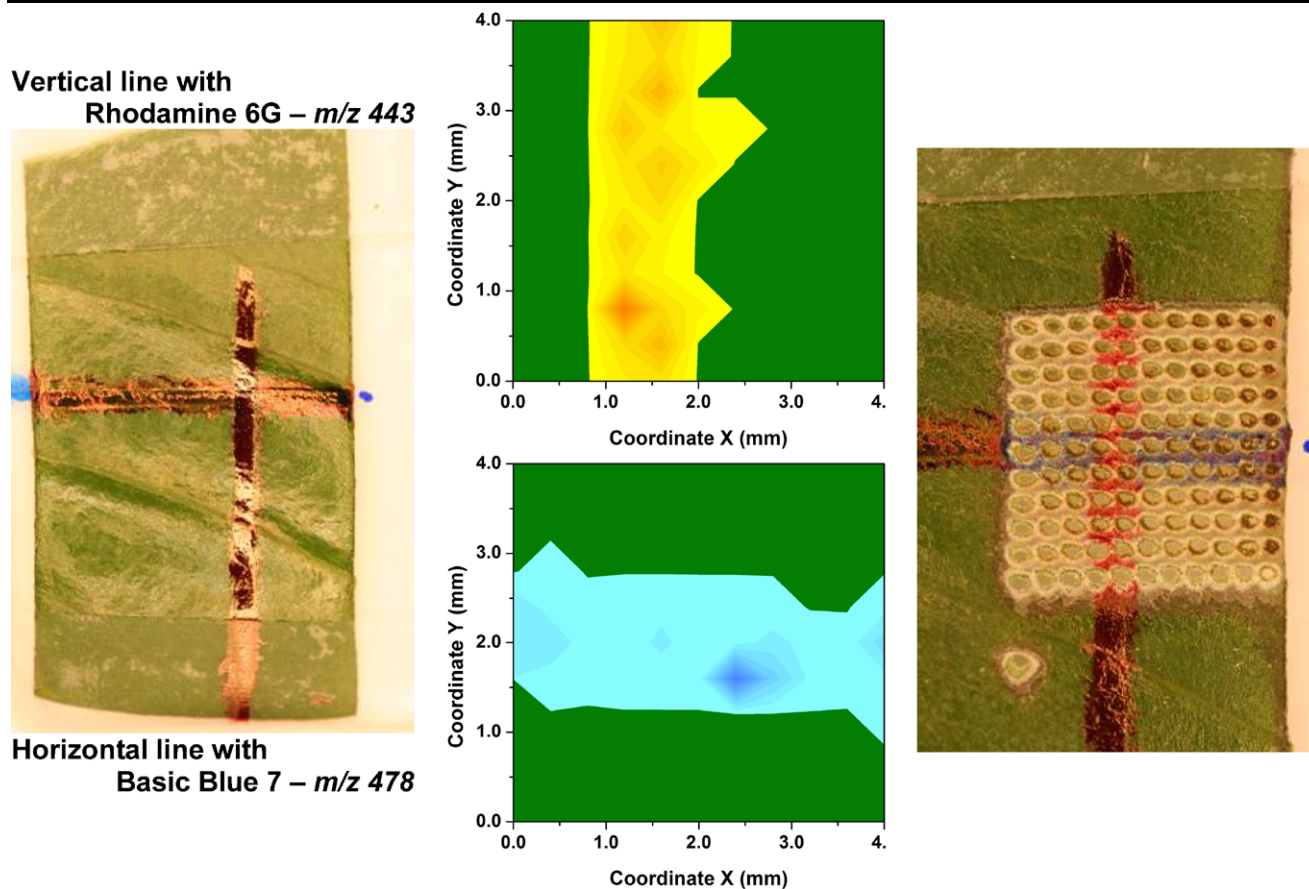


Fig. 4 Imaging of a mock pattern produced on an Peace lily (*Spathiphyllum*) leaf by red (vertical line) and blue (horizontal line) permanent markers. Optical images show the marked leaf section before (left panel) and after (right panel) LAESI imaging. LAESI images for the dye cations indicate a vertical line for the m/z 443 species (Rhodamine 6G in the red marker) (top middle panel) and a horizontal line for the m/z 478 species (Basic Blue 7 in the blue marker) (bottom middle panel)

ter can achieve one to two orders of magnitude higher ion yields. Nevertheless, the complementary nature of the ions detected from plant tissues using the two methods requires further exploration of their utility for any given application.

Acknowledgements This work was supported by the US Department of Energy (DEFG02-01ER15129), by the W.M. Keck Foundation (041904) and in part by the US National Science Foundation (grant No. 0719232). Any opinions, findings, and conclusions or recommendations expressed in this material are those of the authors and do not necessarily reflect the views of the supporting organizations.

References

- D. Gunther, S.E. Jackson, H.P. Longerich, *Spectrochim. Acta B At. Spectrosc.* **54**, 381 (1999)
- R.E. Russo, X.L. Mao, S.S. Mao, *Anal. Chem.* **74**, 70A (2002)
- V.V. Laiko, M.A. Baldwin, A.L. Burlingame, *Anal. Chem.* **72**, 652 (2000)
- M.C. Galicia, A. Vertes, J.H. Callahan, *Anal. Chem.* **74**, 1891 (2002)
- V.V. Laiko, N.I. Taranenko, V.D. Berkout, M.A. Yakshin, C.R. Prasad, H.S. Lee, V.M. Doroshenko, *J. Am. Soc. Mass Spectrom.* **13**, 354 (2002)
- C.E. Von Seggern, R.J. Cotter, *J. Am. Soc. Mass Spectrom.* **14**, 1158 (2003)
- Y. Li, B. Shrestha, A. Vertes, *Anal. Chem.* **79**, 523 (2007)
- C.D. Mowry, M.V. Johnston, *Rapid Commun. Mass Spectrom.* **7**, 569 (1993)
- A. Leisner, A. Rohlfing, U. Rohling, K. Dreisewerd, F. Hillenkamp, *J. Phys. Chem. B* **109**, 11661 (2005)
- H.C. Le, D.E. Zeitoun, J.D. Parisse, M. Sentis, W. Marine, *Phys. Rev. E* **62**, 4152 (2000)
- R. Knochenmuss, L.V. Zhigilei, *J. Phys. Chem. B* **109**, 22947 (2005)
- P.V. Tan, V.V. Laiko, V.M. Doroshenko, *Anal. Chem.* **76**, 2462 (2004)
- B. Spengler, U. Bahr, M. Karas, F. Hillenkamp, *Anal. Instrum.* **17**, 173 (1988)
- K.R. Lykke, P. Wurz, D.H. Parker, M.J. Pellin, *Appl. Opt.* **32**, 857 (1993)
- X.D. Tang, M. Sadeghi, Z. Olumee, A. Vertes, *Rapid Commun. Mass Spectrom.* **11**, 484 (1997)
- P. Voumard, Q. Zhan, R. Zenobi, *Rev. Sci. Instrum.* **64**, 2215 (1993)
- A. Leisner, A. Rohlfing, S. Berkenkamp, F. Hillenkamp, K. Dreisewerd, *J. Am. Soc. Mass Spectrom.* **15**, 934 (2004)
- D.B. Robb, T.R. Covey, A.P. Bruins, *Anal. Chem.* **72**, 3653 (2000)
- J.J. Coon, K.J. McHale, W.W. Harrison, *Rapid Commun. Mass Spectrom.* **16**, 681 (2002)

20. J.J. Coon, W.W. Harrison, *Anal. Chem.* **74**, 5600 (2002)
21. J. Shiea, M.Z. Huang, H.J. Hsu, C.Y. Lee, C.H. Yuan, I. Beech, J. Sunner, *Rapid Commun. Mass Spectrom.* **19**, 3701 (2005)
22. M.Z. Huang, H.J. Hsu, L.Y. Lee, J.Y. Jeng, L.T. Shiea, *J. Proteome Res.* **5**, 1107 (2006)
23. P. Nemes, A. Vertes, *Anal. Chem.* **79**, 8098 (2007)
24. P. Nemes, I. Marginean, A. Vertes, *Anal. Chem.* **79**, 3105 (2007)
25. I. Apitz, A. Vogel, *Appl. Phys. A Mater. Sci. Process.* **81**, 329 (2005)
26. Z.Y. Chen, A. Bogaerts, A. Vertes, *Appl. Phys. Lett.* **89**, 041503 (2006)
27. N. Arnold, J. Gruber, J. Heitz, *Appl. Phys. A Mater. Sci. Process.* **69**, S87 (1999)
28. Y. Li, B. Shrestha, A. Vertes, *Anal. Chem.* **80**, 407 (2008)
29. P. Nemes, A.A. Barton, Y. Li, A. Vertes, *Anal. Chem.* **80**, 4575 (2008)